Crystal Structure of the β-Subunit of Acyl-CoA Carboxylase: Structure-Based Engineering of Substrate Specificity[†,‡]

Lautaro Diacovich,[§] Deborah Lynn Mitchell,[||] Huy Pham,[||] Gabriela Gago,[§] Melrose Mendoza Melgar,[||] Chaitan Khosla,[⊥] Hugo Gramajo,[§] and Shiou-Chuan Tsai*[,||]

Instituto de Biología Molecular y Celular de Rosario (IBR-Consejo Nacional de Investigaciones Científicas y Técnicas) and Departamento de Microbiología, Facultad de Ciencias Bioquímicas y Farmacéuticas, Universidad Nacional de Rosario, Suipacha 531, 2000 Rosario, Argentina, Departments of Chemical Engineering, Chemistry, and Biochemistry, Stanford University, Stanford, California 94305, and Department of Molecular Biology and Biochemistry and Department of Chemistry, University of California, Irvine, California 92612

Received May 8, 2004; Revised Manuscript Received August 2, 2004

ABSTRACT: Acetyl-CoA carboxylase (ACC) and propionyl-CoA carboxylase (PCC) catalyze the carboxylation of acetyl- and propionyl-CoA to generate malonyl- and methylmalonyl-CoA, respectively. Understanding the substrate specificity of ACC and PCC will (1) help in the development of novel structure-based inhibitors that are potential therapeutics against obesity, cancer, and infectious disease and (2) facilitate bioengineering to provide novel extender units for polyketide biosynthesis. ACC and PCC in *Streptomyces coelicolor* are multisubunit complexes. The core catalytic β-subunits, PccB and AccB, are 360 kDa homohexamers, catalyzing the transcarboxylation between biotin and acyl-CoAs. Apo and substrate-bound crystal structures of PccB hexamers were determined to 2.0−2.8 Å. The hexamer assembly forms a ring-shaped complex. The hydrophobic, highly conserved biotin-binding pocket was identified for the first time. Biotin and propionyl-CoA bind perpendicular to each other in the active site, where two oxyanion holes were identified. N1 of biotin is proposed to be the active site base. Structure-based mutagenesis at a single residue of PccB and AccB allowed interconversion of the substrate specificity of ACC and PCC. The di-domain, dimeric interaction is crucial for enzyme catalysis, stability, and substrate specificity; these features are also highly conserved among biotin-dependent carboxyltransferases. Our findings enable bioengineering of the acyl-CoA carboxylase (ACCase) substrate specificity to provide novel extender units for the combinatorial biosynthesis of polyketides.

Acyl-CoA carboxylases (ACCase),[1] such as acetyl-CoA carboxylase (ACC) and propionyl-CoA carboxylase (PCC), catalyze the carboxylation of acetyl-, propionyl-, and butyryl-CoA to provide malonyl-, methylmalonyl-, and ethylmalonyl-CoA, respectively. This carboxylation reaction provides key extender units for the biosynthesis of fatty acids and polyketide natural products (*1*, *2*), which include many antibiotic, anticancer, blood-pressure-lowering, and immunosuppressant compounds (*3*). Furthermore, inhibitors of the ACCases have been identified as potential therapeutics for cancer (*4*−*7*) and obesity (*8*, *9*), as well as potential herbicides and antibiotics (*2*). Very little is known about the molecular basis of ACCase substrate specificity. Understanding ACCase substrate recognition will enable the re-design of the ACCase active site to efficiently synthesize a broader range of substrates for the production of diverse polyketides, as well as structure-based inhibitor design for novel drug discovery.

The reactions catalyzed by ACCase involve two steps and three components (Figure 1A). In the first reaction, the biotin carboxylase (BC) catalyzes the transfer of the carboxyl group to biotin to form carboxybiotin. *In vivo*, biotin is attached to the biotin carboxyl carrier protein (BCCP) via an amide bond between the valeric acid side chain of biotin and the ε-amino group of a lysine on BCCP. In the second reaction, catalyzed by the carboxyltransferase (CT), the carboxyl group is transferred from biotin to acetyl-CoA to form malonyl-CoA. Mammalian, yeast, and most other eukaryotic ACCs are large multifunctional enzymes, containing all three components in one polypeptide chain (*2*). In contrast, three different subunits (BC, BCCP, and CT) compose the *Escherichia coli* ACC (*2*). In actinomycetes, ACCase consists of two polypeptides: an α-subunit containing the BC and BCCP domains and a β-subunit corresponding to the CT domain (*10*). The stoichiometry of the complex subunits was 1:1 as determined in three different studies (*11*−*13*).

Recently, two new ACCases, ACC and PCC, have been characterized from *Streptomyces coelicolor* (*10*, *14*, *15*).

[†] Part of this work was supported by a Fogarty International Research Collaboration Award from the NIH to C.K. and H.G. (R03 TW005778) and by ANPCyT Grant 01-06622 to H.G.

[‡] The atomic coordinates have been deposited in the Protein Data Bank (entries 1X06, 1XNV, 1XNY, and 1XNW).

* To whom correspondence should be addressed. Phone: (949) 824-4486. Fax: (949) 824-8552. E-mail: sctsai@uci.edu.

[§] Universidad Nacional de Rosario.

[||] University of California, Irvine.

[⊥] Stanford University.

[1] Abbreviations: ACCase, acyl-CoA carboxylase; ACC, acetyl-CoA carboxylase; PCC, propionyl-CoA carboxylase; PKS, polyketide synthase; AccB, β-subunit of ACC; PccB, β-subunit of PCC; AccE, ε-subunit of ACC; PccE, ε-subunit of PCC; AccA2, α-subunit of ACC or PCC.

10.1021/bi049065v CCC: $27.50
Published on Web 11/02/2004

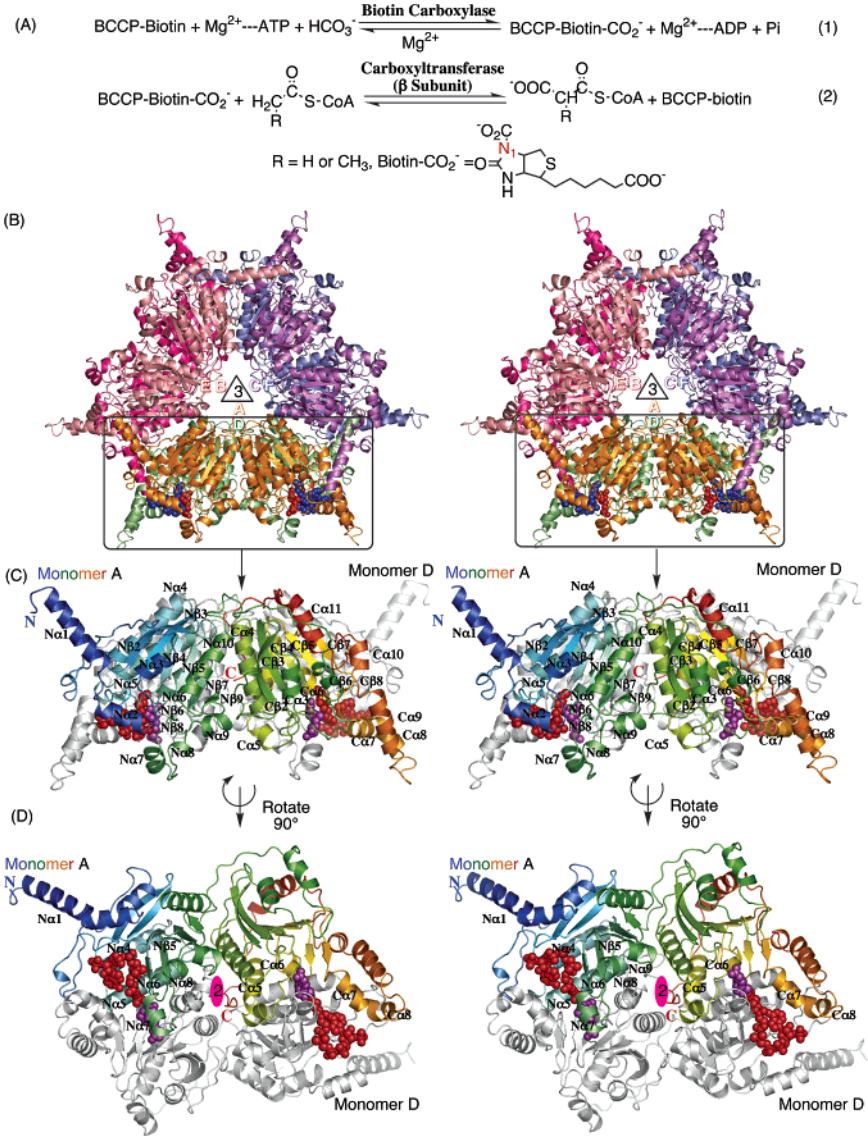

FIGURE 1: (A) Two-step reactions of ACCase. (B) Overall hexameric structure of PccB. The hexamer has 32 symmetry; specifically, it forms two stacks of three monomers (A−B−C and D−E−F) related by the 3-fold axis (indicated by the triangle), while A−D, B−E, and C−F monomers form three tightly interacting dimers related by the 2-fold axis shown in panel D. (C) Monomer A of PccB, colored from the N-terminus (blue) to the C-terminus (red), with two structurally similar domains (N and C). Monomer D is shown in black and white under monomer A. (D) Monomers A (in rainbow) and D (in white) after a 90° rotation. The helices from the N-domain (N-α5, N-α6, and N-α7) of monomer A interact with the corresponding helical regions in the C-domain (C-α5 and C-α6) of monomer D. The 2-fold axis is shown in purple. The di-domain, dimeric interaction is ubiquitously important for enzyme catalysis, substrate recognition, and protein stability of biotin-based carboxyltransferases.

ACC and PCC were shown to be involved in fatty acid and polyketide biosynthesis. Heterologous expression of the *S. coelicolor* PCC complex in *E. coli* has enabled the biosynthesis of methylmalonyl-CoA, a metabolite that does not normally accumulate in *E. coli*, and the production of the polyketide 6-deoxyerythronolide B when coexpressed with the erythromycin PKS (*16*). More generally, successful production of polyketide compounds in heterologous hosts depends on enhancing the biosynthesis of extender units such as methylmalonyl-, malonyl-, and ethylmalonyl-CoA, typically via ACCase overexpression or engineering. Therefore, understanding the basis of ACCase substrate recognition will facilitate the generation of ACCase *a la carte* for the production of pharmacologically important polyketides.

Significantly, an extra subunit, ϵ, was found for ACC and PCC in *S. coelicolor*, whose role appears to be important for formation of the complex (*15*). Both enzyme complexes share the same biotinylated subunit, AccA2. However, the β- and ϵ-subunits are specific. Thus, for the PCC complex, the β- and ϵ-subunits are designated PccB and PccE, and AccB and AccE for ACC. While ACC was able to carboxylate acetyl-, propionyl-, or butyryl-CoA with approximately the same specificity, the PCC complex could not recognize acetyl-CoA as a substrate (*10*, *14*, *15*). Considering that both complexes share the same α-subunit (AccA2), the substrate acyl-CoA recognition should reside in the β-chain (AccB and PccB). However, very little is known about the molecular basis that leads to the different specificity in ACC and PCC.

Sequence alignment indicates that AccB and PccB belong to the family of carboxyltransferases that use biotin as the CO_2 carrier (*17*). Three biotin-dependent carboxyltransferase structures have been determined, including yeast-CT (for acetyl-CoA carboxylation) (*18*), glutaconyl-CoA decarboxylase (for sodium ion pump) (*19*), and transcarboxylase 12S

(for pyruvate carboxylation) (*20*); their sequences are 15, 23, and 51% identical with that of PccB, respectively. Both yeast-CT and glutaconyl-CoA decarboxylase are dimers (*18*, *19*), while 12S (catalyzes the reverse reaction of the hexameric PccB) is a hexamer (*20*). Although each protein has a different cellular function, they all consist of two domains (N and C). Each domain contains a crotonase fold (*21*) that is also found in 4-chlorobenzoyl-CoA dehalogenase (*22*), MMCoA decarboxylase (*23*), enoyl-CoA hydratase (*24*), and dienoyl-CoA isomerase (*25*). Except for MMCoA decarboxylase, the active site is proposed to be located at the dimeric interface (*21*). While these structures provide important steps toward understanding this important family of enzymes, many key questions remain to be answered, such as how biotin binds to biotin-dependent carboxyltransferases or how acetyl-CoA can be differentiated from propionyl- or butyryl-CoA.

To provide further insight into these questions, we have determined the crystal structure of the apo and substrate-bound β-subunit of PCC (PccB) from *S. coelicolor*. Significantly, both the biotin binding pocket and the acyl-CoA binding pocket were identified, providing a structural basis for the proposed mechanism. On the basis of the amino acid sequence alignment, the propionyl-CoA-bound structure, and structure comparison between AccB and PccB, the molecular basis of substrate specificity was also investigated by structure-based mutations. Our structural and functional studies indicate that the dimeric, di-domain interaction, crucial for enzyme catalysis, stability, and substrate specificity, should be ubiquitous among biotin-dependent carboxyltransferases.

MATERIALS AND METHODS

Chemicals, Strains, and DNA Manipulation. *E. coli* strain DH5α was used for routine subcloning and transformed according to the method of Sambrook *et al.* (*10*). Transformants were selected on media supplemented with the appropriate antibiotics (100 μg/mL Ap, 20 μg/mL Cm, or 50 μg/mL Km). Strain BL21 λ(DE3) is an *E. coli* B strain lysogenized with λDE3, a prophage that expresses the T7 RNA polymerase from the IPTG-inducible *lac*UV5 promoter (*2*). Rosetta λ(DE3) expresses rare tRNAs to facilitate expression of genes that encode rare *E. coli* codons.

Expression and Purification. Recombinant AccA2, AccB, PccB, AccE, and PccE were expressed in *E. coli* and purified as described to yield >95% pure protein (*10*). The buffer was exchanged with 10 mM HEPES (pH 7.0) and 2 mM dithiothreitol (DTT) by a Pharmacia PD-10 desalting column and concentrated with a Centricon YM-10 concentrator to 4−20 mg/mL. The enzyme assays were performed as described previously (*10*).

Mutagenesis of D422I PccB and I420D AccB. Site-directed mutations were introduced into both CTs by a PCR-based method with two rounds of PCR. The I420D mutation in AccB was introduced with the ABIDdown primer (5′-GGACTGGCTGTCCATGACGTCGTAAGCACCTCCGT-ACGCC-3′). The other two primers used in the mutagenesis protocol were NaccB (5′-TATTCTAGACATATGACCGT-TTTGGATGAGG-3′), containing an *Nde*I site (underlined) that anneals to the 5′ end of the *S. coelicolor accB* gene, and the CaccB primer (5′-ATAGAATTCTCACTGCG-GCGGGTTG-3′) that introduces an *Eco*RI site (underlined) at the translational stop codon of the gene. A first round of PCR was carried out using Pfu polymerase (Promega), primers NAccB and ABIDdown, and pTR90 as the template. The PCR product was purified and used with oligonucleotide CAccB for a second round of PCR. The resulting amplified fragment (mutated accB) was cloned into the Topo blunt vector (Promega), yielding pL34. To generate a His tag fusion protein, an *Nde*I−*Hin*dIII fragment from pL34 was cloned into an *Nde*I−*Hin*dIII-cleaved pET28a(+) (Novagen), yielding pL39. The D422I PccB mutant was constructed with a similar approach. The primers utilized were PBDIdown (5′-GGTGCTTGGAGCCCATGACGATGTAG-GCGCCGAAGGC-3′) that introduces the two-base mutation, NPccB (5′-TATCTAGACATATGTCCGAGCCGGAAGAG-3′) that introduces an *Nde*I site (underlined) at the translational start codon of the *S. coelicolor pccB* gene, and CPccB (5′-ATAGAATTCTTACAGGGGGATGTTG-3′) that introduces an *Eco*RI site at the translational stop codon of the gene. The mutated *pccB* gene was cloned into Topo blunt vector (Promega), yielding pL35, and then passed onto pET28a(+) (Novagen) as an *Nde*I−*Hin*dIII fragment to generate pL40, which expresses the His tag fusion protein. Both mutations were verified by DNA sequencing.

Crystallization of PccB. Crystals of PccB were grown in sitting drops at room temperature by vapor diffusion. The protein buffer consisted of 10 mM HEPES (pH 7.0) and 2 mM DTT. Drops were generated by mixing 2 μL of the purified protein solution with 2 μL of well buffer above 500 μL of well solution. Three crystal forms of PccB were grown at 7 mg/mL. For the cocrystallization experiment, 5 mM propionyl-CoA and 10 mM biotin were mixed with 10 mg/mL PccB. The crystallization conditions for each crystal form are listed in Table 1.

Data Collection. X-ray diffraction data of PccB were collected at the Advanced Light Source (ALS) to 2.0−3.3 Å (Table 1). Crystals were frozen accordingly in different crystal forms (Table 1), mainly in 30% glycerol and 70% well solution. The crystal space groups and cell dimensions are listed in Table 1. The concentrations of the substrate cocrystal are 10 mM biotin and 5 mM propionyl-CoA. Diffraction intensities were integrated, reduced using DENZO, and scaled using SCALEPACK (*26*). A summary of the crystallographic data is given in Table 1.

Molecular Replacement and Refinement. Initial phases were determined by molecular replacement, using the crystal structure of 12S as the search model (PDB entry 1ON3). A cross-rotational search followed by a translational search was performed utilizing CNS (*27*). After the structure had been rebuilt using Quanta, further refinement was performed using CNS (*27*). The noncrystallographically related monomers were treated as rigid bodies and were refined using CNS to give an initial R_{crys} of 42%. A preliminary round of refinement using torsion angle simulated annealing, followed by energy minimization and positional and individual *B*-factor refinement, reduced R_{crys} to 29%. Subsequent rounds of model building and refinement were carried out using the maximum likelihood-based approach implemented within CNS using all data to the highest resolution. Strict noncrystallographic symmetry restraints were applied for the first round of refinement and then released for subsequent model building of each monomer. Refinement was continued to an

Table 1: Crystallization, Data Collection, and Refinement Statistics

	apo-PccB-1	apo-PccB-2	biotin-PrCoA-PccB	D422I PccB
Crystallization				
	0.22 M magnesium formate	1.4 M sodium citrate at pH 5.5	1.4 M sodium citrate at pH 5.6	35% MPD Bis-Tris at pH 6.0
Crystallographic Data				
space group	$P2_12_12_1$	$P6_3$	$P6_3$	$P2_1$
cell dimensions	86.90 Å, 178.98 Å, 296.30 Å, $\alpha = \beta = \gamma = 90°$	166.94 Å, 166.94 Å, 80.49 Å, $\alpha = \beta = 90°$, $\gamma = 120°$	166.74 Å, 166.74 Å, 79.22 Å, $\alpha = \beta = 90°$, $\gamma = 120°$	79.85 Å, 219.49 Å, 135.69 Å, $\alpha = \gamma = 90.0°$, $\beta = 102.9°$
resolution (Å)	2.0	2.3	2.0	2.6
mosaicity (deg)	0.4	0.4	0.4	1.0
no. of observations	3369767	879802	2372095	1455643
no. of unique reflections	510544	111570	137644	139417
completeness (last shell) (%)	92.4 (92.0)	99.5 (93.6)	99.2 (97.2)	100.0 (99.4)
$I/\sigma(I)$ (last shell)	11.2 (2.2)	19.0 (3.4)	33.5 (7.2)	8.5 (1.4)
R_{merge} (last shell) (%)	8.6 (53.2)	12.9 (49.1)	10.3 (32.3)	12.6 (78.9)
no. of refinement reflections	201135	53953	82540	122262
no. of protein atoms	23718	7906	7905	23664
no. of cofactor atoms	0	0	136	0
no. of waters	1923	706	817	387
R_{free} (%)	24.5	22.4	22.8	26.0
R_{crys} (%)	20.8	18.6	19.0	24.1
Geometry				
rmsd for bonds (Å)	0.0060	0.0060	0.0054	0.0095
rmsd for angles (deg)	1.27	1.26	1.26	1.24
rmsd for *B* (main chain)	1.21	1.19	1.19	1.20
rmsd for *B* (side chain)	2.07	2.15	2.09	2.17
Ramachandran plot (%)				
most favored	89	92	93	93
favored	10	7	6	5
generously allowed	1	1	1	2

R_{crys} of <25% (R_{free} < 27%). Table 1 lists the statistics for refinement and components of the final model. After the R_{free} decreased below 0.27, water molecules were added using CNS, followed by visual inspection of the water molecules and final refinement of the *B*-factor.

RESULTS AND DISCUSSION

Overall Fold. Three crystal structures were determined: the apo 360 kDa hexameric structure of wild-type PccB (two crystal forms), the substrate-bound (biotin and propionyl-CoA) wild-type PccB, and the D422I mutant of PccB. Different crystal forms of PccB (with an overall rmsd of <0.6 Å) yield the same hexameric, ring-shaped architecture with overall dimensions of 150 Å × 110 Å × 50 Å, while the internal pore size ranges from 10 to 20 Å (Figure 1B). The hexamer stoichiometry of AccB and PccB is consistent with dynamic light scattering measurements and size-exclusion chromatography (data not shown). By inference, from examples in the literature, the stoichiometry of the complex subunits should be 1:1 (*11*−*13*). Therefore, our studies imply an overall $\alpha_6\beta_6\epsilon_{>6}$ stoichiometry for the holo ACC and PCC complexes, with an overall molecular weight of >1 MDa.

Similar to the *Propionibacterium shermanii* 12S transcarboxylase that was used for molecular replacement (*20*), the PccB hexamer has a 32-fold symmetry, where a 3-fold axis (Figure 1B) is perpendicular to a 2-fold axis (Figure 1D). Specifically, A−B−C and D−E−F monomers form two tightly interacting trimer rings (Figure 1B), while A−D, B−E, and C−F dimers interact extensively (Figure 1D). Only minor differences are observed among the six monomers, with an rmsd of <0.5 Å. Like 12S and yeast-CT (*18*, *20*), PccB also reveals two domains (N- and C-domains) in each monomer, and both domains have a crotonase fold that consists of seven β-sheets and α-helices (Figure 1C). Although the sequences of N- and C-domains are less than 12% identical, the backbone rmsd is <1.5 Å. This suggests an ancient gene duplication event that resulted in the di-domain structure. Indeed, sequence comparison reveals that the two subunits (α and β) of the carboxyltransferase in *E. coli* correspond to the C- and N-domains in PccB, respectively (*2*). The domain repetition is crucial for the molecular recognition properties of carboxyltransferases.

The intertrimer interactions (A−B−C to D−E−F), as well as the six active sites, are located at the interface of the N-domain of one monomer and the C-domain of its dimeric partner (Figure 1C,D). Specifically, the helices from the N-domain (N-α5, N-α6, and N-α7) of one monomer interact with the corresponding helical regions in the C-domain (C-α5 and C-α6) of its dimeric partner. Intertrimer (A−D, B−E, and C−F monomers) interactions include the following: D530−R392, N527 (C═O)−R358, N527 (NH)−S167, N527−T362 or −D192, H525−D364, K524−D364, and P522 (C═O)−N262 (Figure 2). In addition, intratrimer interaction (for example, between monomers A and B) occurs mainly between the C-terminal helices of one monomer and N-terminal helices of its trimeric partner (Figures 1B and 3B). The overall structure illustrates the importance of interdomain interactions for the activity and stability of carboxyltransferases such as 12S, yeast-CT, AccB, and PccB.

Surface Charge Differences. Although the overall structures of PccB and 12S are similar (rmsd = 0.86 Å), there are several key differences. Whereas 12S has a calculated net charge of −64 at pH 7.0 (20), the surface of PccB is even more electronegative than the 12S surface, with a calculated net charge of −120 at pH 7.0 (Figure 3A). In

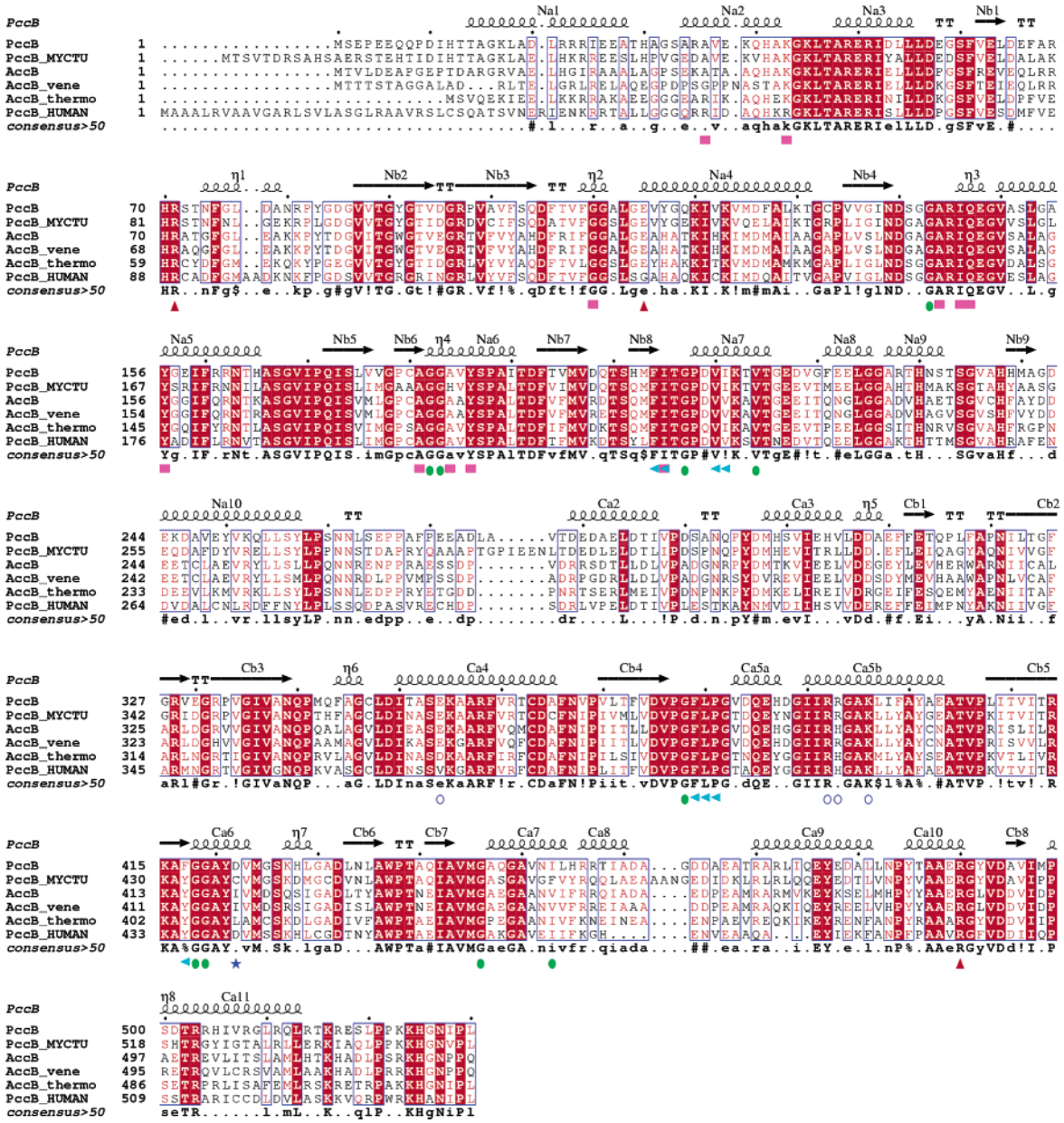

FIGURE 2: Sequence alignment of carboxyltransferases PccB-MYCTU, AccB_vene, AccB_thermo, and PccB_HUMAN: PccB from *Mycobacterium tuberculosis*, AccB from *Streptomyces venezuelae*, AccB from *Thermoanaerobacter tengcongensis*, and PccB from human. Legend: red triangle, residues important for dimer−dimer interaction; blue star, residue 422; black circle, highly conserved G and V at the dimeric, di-domain interface; purple bar, residues important for acyl-CoA binding; green triangle, residues important for biotin binding; #, conserved hydrophilic residues; ! and $, conserved hydrophobic residues; %, conserved aromatic residues.

addition, on the basis of the hexameric crystal structures of PccB, a homology model of AccB was generated using SwissModel (*28*), revealing a much less electronegative surface (Figure 3A). The large difference in surface properties among AccB, PccB, and 12S may reflect a major difference in protein−protein interaction. Although AccB and PccB accept carboxylated biotin from the upstream AccA2, they interact with different adapter proteins, AccE and PccE, respectively. AccE and PccE both have a positive calculated charge at pH 7.0 (3.6 for AccE and 1.9 for PccE). Because AccA2 is also highly electronegative, with a calculated net charge of −20 per monomer, the ϵ-subunit can be the adapter molecule between the highly electronegative α- and β-subunits. The intersubunit interaction of AccA2−AccB−AccE versus that of AccA2−PccB−PccE may be highly specific for each complex. Indeed, there is no catalytic reaction upon prolonged incubation of substrates with AccA2, AccB, and PccE (or AccA2, PccB, and AccE), indicating the highly specific nature of intersubunit interaction (*10*). It is likely that the differences in surface recognition, i.e., protein−protein interactions, reflect the differences in their corresponding biochemical roles.

Hexamer versus Dimer. Because the oligomeric state of ACCase may be related to its metabolic regulation (*1*), it is interesting to compare the dimeric structures of yeast-CT and glutaconyl-CoA decarboxylase (GCD) (*18*, *19*) with the hexameric structures of PccB and 12S. Although the level of sequence identity between yeast-CT and PccB is <15%, structural alignment revealed that the relative orientation and distance between the N- and C-domains are very similar, and the secondary structures are also well aligned, resulting in an rmsd of only 1.5 Å between the main crotonase fold

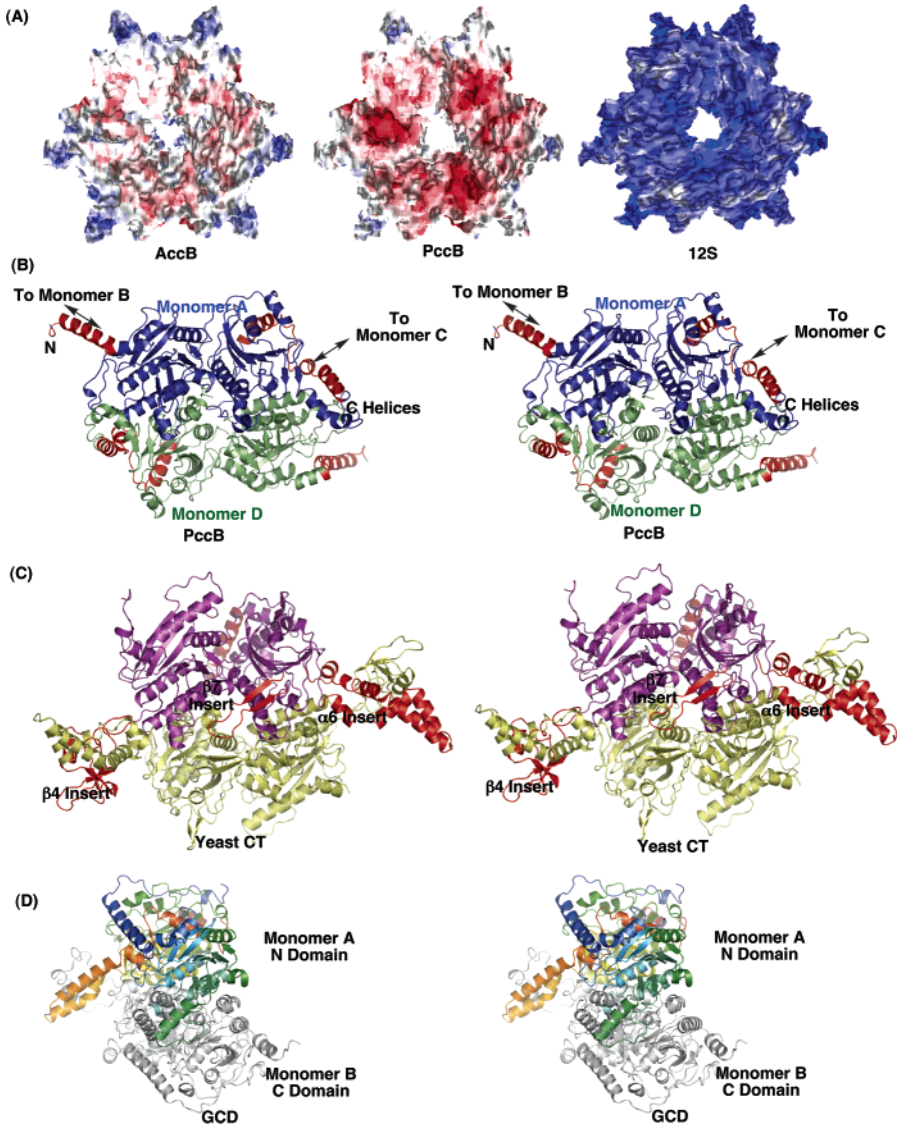

FIGURE 3: (A) Electronegative surfaces of AccB, PccB, and 12S reveal key differences between these very similar carboxyltransferases, indicating their different biological receptors. Surfaces are colored from red (−15 keV) to white (−7 keV) to blue (1 keV). (B) C- and N-helical regions of PccB (in red for both monomers) that are important for hexamer formation. Monomers A and D are colored blue and green, respectively. (C) The dimeric structure of yeast-CT (monomers A and D in purple and yellow) indicates extra dimeric interaction from the inserted regions (in red for monomer A), while C-terminal helical regions (in red) prevent yeast-CT from forming a hexamer. (D) Dimeric structure of GCD (monomer A in rainbow from the N- to C-terminus, monomer B in white). Although the di-domain arrangement within the monomer is very different (the C-domain of monomer A is oriented away from the viewer), the di-domain, dimeric interaction is still very similar among GCD, yeast-CT, and PccB.

region (Figure 3C). The interactions between the N-domain of one monomer (N-α5, N-α6, and N-α7, numbering according to this work) and the C-domain of its dimeric partner are very similar between yeast-CT and PccB, despite the low level of sequence homology. Similarly, the di-domain, dimeric interaction is also observed in the dimeric structure of GCD (Figure 3D), although its N-domain and C-domain arrangement is completely different from that of PccB and 12S (*19*). Such a similarity highlights the importance of maintaining the dimeric, di-domain interaction for carboxyltransferases.

The major difference between yeast-CT and PccB lies in the insertion regions of yeast-CT, which has a large β-insertion at the N-domain, one β-insertion and one α-helical insertion at the C-domain, and an additional four-helix region at the C-terminus (Figure 3C). As a result, the four additional α-helices at the C-terminus of yeast-CT prevent it from forming a hexamer as in the case of PccB or 12S (Figure 3B). Sequence alignment of different dimeric carboxyltransferases reveals that the C-terminal α-helices as well as the insertions are ubiquitous features for dimeric carboxyltransferases (*18*), but not for hexameric ones such as AccB, PccB, or 12S.

Active Site. The active site of PccB was identified on the basis of the electron density maps ($2|F_o| - |F_c|$ omit maps) of propionyl-CoA and biotin (Figure 4A). This provides us with a first glimpse of the biotin−protein interactions for biotin-dependent carboxyltransferases. The acyl-CoA binding pocket and the biotin pocket are both located at the interface between the N-domain of one monomer and the C-domain of its dimeric partner (Figure 1C,D). Loops between N-β3 and N-α4, N-β4 and N-α5, N-β5 and N-α6, C-β5′ and C-α6′, and C-β7′ and C-α7′ define the coenzyme A binding pocket, while loops between N-β6 and N-α7, C-β5′ and C-α6′, and

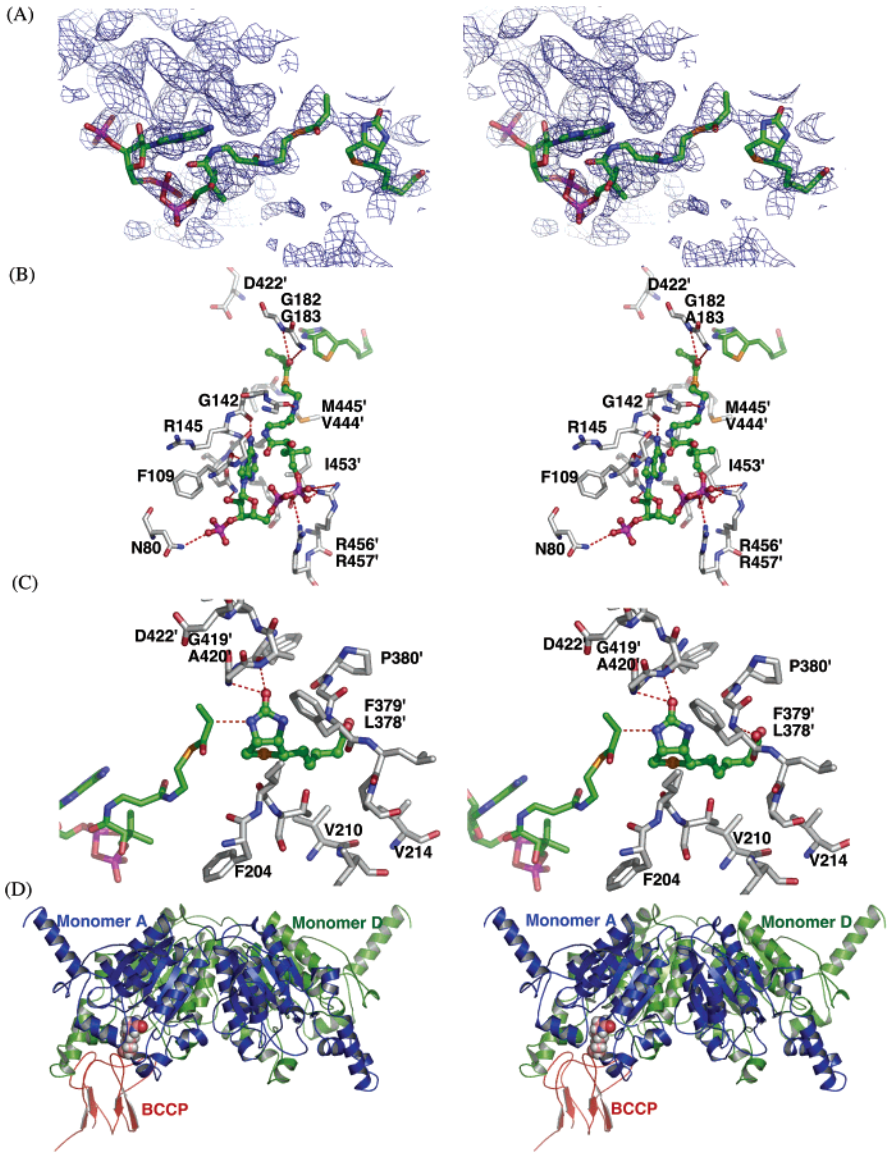

FIGURE 4: (A) Omit $2F_o - F_c$ electron density maps of biotin and propionyl-CoA in the active site. (B) The binding pocket of propionyl-CoA reveals that residue 422, at the end of the pocket, is the only residue different in AccB and PccB. Hydrogen bonds between propionyl-CoA and the protein are represented by red dashed lines. The carbonyl group of propionyl-CoA forms hydrogen bonds with the NH groups of G182 and G183 (the proposed first oxyanion hole). (C) Hydrophobic binding pocket of biotin with highly conserved aromatic and hydrophobic residues. Hydrogen bonds between propionyl-CoA and the protein are represented by red dashed lines. Significantly, N1 of biotin and the C-α of propionyl-CoA are 3.4 Å away, enabling α-hydrogen abstraction by N1. The carbonyl group of biotin forms hydrogen bonds with the NH groups of G419′ and A420′ (the proposed second oxyanion hole). (D) Docking simulation between PccB (monomers A and D in blue and green) and the homology model of the BCCP domain of AccA2 (in red). A cleft region in PccB was found to match the shape of the loop region that contains the lysine−biotin−carboxylate flexible arm. Biotin is shown as a sphere.

C-β7′ and C-α7′ define the biotin binding pocket. The binding pockets of acyl-CoA and biotin are perpendicular to each other and meet at the junction of the L-shaped active site, near the intersection of N-β5 and N-α6 of one monomer and C-β5 and C-α6 of its dimeric partner (Figure 1C,D). The cocrystal structure shows that acyl-CoA binds predominantly to one domain (e.g., C-domain) of the first monomer, while biotin binds to the alternate domain (e.g., N-domain) of its dimeric partner and meets acyl-CoA at the dimer interface. Such a dimeric, di-domain active site arrangement is conserved across the biotin-dependent carboxyltransferases, including 12S (*20*), GCD (*19*), and yeast-CT (*18*).

The biotin−streptavidin interaction is one of the strongest ligand−protein interactions in biological systems (*29*, *30*), with a binding constant of 10^{-15} M^{-1}. The biotin−streptavidin interaction was found to be predominantly hydrophobic and van der Waals in nature, with many aromatic residues involved in binding (*30*). From the cocrystal structure, the biotin−PccB interaction is also predominantly hydrophobic in nature and highly conserved: residues that line the biotin binding pocket include highly conserved F379, L380, P381, and F417 of one monomer and F204′, I205′, V210′, and I211′ of its dimeric partner (Figures 2 and 4C). In addition, the position of the ureido moiety of biotin points to two possible oxyanion holes, which become the basis of the proposed enzymatic mechanism elaborated below.

Previously, a mutational study has investigated the active site of the carboxyltransferase domain of pyruvate carboxylase (*31*). K712 and D543 were identified as the key acid and base catalysts, respectively. However, these two residues are conserved in AccB and PccB (corresponding to Q199 and A36, respectively), and they map to the surface of PccB

Table 2: Kinetics of Wild-Type and Mutant AccB and PccB Reacting with Acetyl-, Propionyl-, and Butyryl-CoA[a]

	acetyl-CoA			propionyl-CoA			butyryl-CoA		
complex (5 μg)	K_m (μM)	V_{max} [milliunits min^{-1} (mg of AccA2)$^{-1}$]	specificity constant V_{max}/K_m	K_m (μM)	V_{max} [milliunits min^{-1} (mg of AccA2)$^{-1}$]	specificity constant V_{max}/K_m	K_m (μM)	V_{max} [milliunits min^{-1} (mg of AccA2)$^{-1}$]	specificity constant V_{max}/K_m
AccA2−AccB−AccE[b]	100 ± 22	432 ± 27	4.3	92 ± 10	620 ± 21	6.7	99 ± 12	439 ± 17	4.4
AccA2−PccB−PccE[b]	NR[c]	NR[c]	−	76 ± 5	1063 ± 21	13.9	104 ± 27	690 ± 65	6.6
AccA2−I420D−AccE	NR[c]	NR[c]	−	310 ± 61	463 ± 33	1.5	NR[c]	NR[c]	−
AccA2−D422I−PccE	335 ± 46	470 ± 23	1.4	315 ± 52	1006 ± 62	3.2	317 ± 30	832 ± 27	2.6

[a] The enzyme activity was determined by the protocol described in ref *10*. Briefly, the production of ADP was coupled to pyruvate kinase and lactate dehydrogenase, and the oxidation of NADH was followed at 340 nm. The assay mixture contained 5 units of pyruvate kinase, 10 units of lactate dehydrogenase, 0.5 mM phosphoenolpyruvate, 0.2 mM NADH, 5 mM $MgCl_2$, 0.3 mg/mL BSA, 100 mM potassium phosphate (pH 7.6), 3 mM ATP, 50 mM $NaHCO_3$, and the appropriate concentrations of acyl-CoA. Reactions were initiated by addition of the different enzyme components. [b] The wild-type kinetic data were taken from ref *10*. [c] No detectable activity.

that is far from the active site. Therefore, the active site identified in this study must be very different from the one found in the pyruvate carboxylase mutagenesis.

The binding motif and coenzyme A conformation of propionyl-CoA are very similar to those observed for 12S and yeast-CT (Figure 4B) (*18*, *20*). Residues in the acyl-CoA binding pocket are also highly conserved among di-subunit CTs (Figure 2). Therefore, on the basis of the substrate biotin−propionyl-CoA cocrystal structure of PccB and the comparison with the structures of 12S, GCD, and yeast-CT, the motif of binding of acyl-CoA and biotin to CT should be ubiquitous among biotin-based carboxyltransferases, where dimeric, di-domain interactions are crucial for its activity.

Substrate Specificity. The molecular basis of substrate specificity, i.e., how the enzyme differentiates acetyl-CoA from propionyl-CoA, remains an important open question. Previous kinetic study on AccB and PccB used three different assays and confirmed that wild-type AccB accepts acetyl-, propionyl-, and butyryl-CoA as its substrates (Table 2 and ref *10*), while PccB accepts propionyl- and butyryl-CoA but not acetyl-CoA. The observed substrate specificity has been discussed in the context of the biological role of ACC and PCC in *S. coelicolor*, that ACC may be involved in both fatty acid and actinorhodin polyketide biosynthesis, while PCC may provide methylmalonyl-CoA for the biosynthesis of other polyketides associated with *S. coelicolor* (*10*). However, the molecular basis of the substrate specificity is not understood.

To understand the molecular basis of substrate specificity, the active sites of the AccB (homology model) and PccB structures were compared. Significantly, nearly all residues in the acyl-CoA binding pocket are conserved (Figure 2), except residue 422 of PccB (420 in AccB) that is located at the end of the acyl-CoA binding pocket (Figure 4B). Residue 422 is an Asp in PccB and an Ile (420) in AccB. Sequence comparison indicates that for different CTs that accept propionyl-CoA as a substrate, including *S. coelicolor* PccB and human PccB, this position is occupied by small residues, such as Asp or Cys (Figure 2). On the other hand, for CTs that accept acetyl-CoA as a substrate, such as AccB, this residue is a larger, hydrophobic residue (Figure 2). We hypothesized that the amino acid property of this position may help to define the shape of the acyl-CoA binding pocket.

Two mutants were made from the two ACCases that were being studied to test this hypothesis, one for PccB (D422 to I422) and the second for AccB (I420 to D420). The crystal structure of the PccB D422I mutant is very similar to the wild-type structure (Table 1), indicating no changes in conformation under the crystallization conditions that were used. The AccB and PccB mutants provided important information: wild-type PccB does not accept acetyl-CoA as its substrate, presumably due to a larger acyl-CoA binding pocket and different hydrogen bonding network around the active site that does not properly interact with the two-carbon acetyl group. If residue 422 is the key to substrate recognition, the D422I mutant of PccB should accept acetyl-CoA because of its more compact and hydrophobic substrate-binding pocket. As predicted, the PccB D422I mutant not only accepted acetyl-CoA as its substrate but also exhibited substrate specificity similar to that of wild-type AccB for propionyl- and butyryl-CoA (Table 2). Furthermore, the AccB I420D mutant cannot accept acetyl-CoA as its substrate (Table 2). In essence, by a single mutation in the proposed active site, the substrate specificities of mutant ACC and PCC have been interchanged.

Additionally, the I420D AccB mutant also does not recognize butyryl-CoA as a substrate (Table 2). This implies the involvement of surrounding active site residues in substrate recognition of AccB. Our results confirm that acyl-CoA specificity is indeed determined by the CT domain of the multisubunit complex and provide a molecular basis of substrate recognition for ACCases.

Protein−Protein Docking between the α- and β-Subunits. With the identification of the biotin binding pocket, it is of great interest to understand how the BCCP domain of AccA2, which transports carboxylbiotin, may interact with AccB or PccB. Both AccB and PccB accept CO_2 via carboxylbiotin linked to a BCCP lysine ϵ-amide bond, corresponding to K122 in *E. coli* BCCP (*32*). The NMR structure of the latter indicates that K122 is located in a dynamic loop region (*2*). The loop region is capable of transporting the carboxylbiotin moiety with a long, sweeping arm that consists of the loop, lysine 122, and biotin itself. A homology model of the BCCP domain of AccA2 was generated using the *E. coli* BCCP structure, and protein−protein docking was simulated using 3D-Dock (*33*). All of the highest scores point to a binding cleft of PccB that matches the loop regions of BCCP very well (Figure 4D). This cleft is also dimeric, di-domain in nature, consisting of C-α7, C-α8, N-α7, and N-α8 of both monomers. Protein−protein interaction is hydrophilic in nature with an extensive hydrogen bonding network (Figure 4D). The simulated binding motif between BCCP and PccB, combined with the open L-shaped binding pocket of biotin

and propionyl-CoA, allows the lysine−biotin arm of BCCP to sweep through a large radius, alternatively reaching between the active site of PccB and AccA2.

Proposed Mechanism and Biological Significance. Previous pH-dependent kinetic studies on *E. coli* CT indicated the presence of an active site base with a pK_a of 8.0, implicating cysteine as the active site base (*34*). However, as in the yeast-CT and 12S structures, there is no cysteine in the active site of PccB. The identification of the active site base is important for the elucidation of the enzyme mechanism and drug design, and becomes a key issue in the enzyme catalysis of CTs.

In this work, the biotin-bound structure of PccB supports the proposal that the active site base is biotin itself, which has been previously proposed for GCD and yeast-CT (*18*, *19*). At the end of the binding pocket, the biotin carbonyl group forms hydrogen bonds with the backbone amide nitrogen of G419′ and A420′, providing a suitable oxyanion hole that can stabilize a ureido anion upon deprotonation of N1 (Figure 4C). Further, N1 of biotin is in the proximity (3.5 Å) of the C-α atom of propionyl-CoA and is hydrogen-bonded to the carbonyl group of propionyl-CoA (Figure 4C). In addition, past studies indicate that N1 can be readily deprotonated ($>10^{12}$ s^{-1}) at pH 7.0 (*29*). Therefore, N1 of biotin is well-positioned and electronically capable of deprotonating propionyl-CoA.

On the basis of the crystal structures of wild-type and mutant PccB and AccB, as well as the substrate-bound structure and docking simulation, we propose the following catalytic mechanism for the carboxyltransferase PccB and AccB (Figure 5). PccB forms a ring-shaped hexamer with a highly electronegative surface. AccA2, also highly electronegative, can bind to either the top or the bottom of the PccB hexamer, presumably with docking assistance from the electropositive ϵ-subunits. The BCCP domain of AccA2 is bound to PccB at a highly complementary surface, allowing the lysine−biotin arm to transfer the carboxyl group between the active sites of the BC domain and PccB. On the basis of previous theoretical calculation (*29*), upon binding the carboxylbiotin moiety to the enzyme, CO_2-biotin can be destabilized by enzyme-induced bending of the CO_2−N1−CO−N π orbital, resulting in the loss of CO_2 from biotin. The release can be stabilized by the oxyanion hole at G182 and G183 (Figure 4B), while the resulting ureido enolate in biotin can be stabilized by the oxyanion hole at G419′ and A420′ (Figure 4C). Subsequent deprotonation of the α-carbon of propionyl-CoA results in the propionyl enolate, which can be stabilized by the G419′−A420′ oxyanion hole. The attack of the propionyl enolate on CO_2 then produces the product methylmalonyl-CoA. Although a concerted mechanism is possible, the above stepwise mechanism (with the release of CO_2) is proposed on the basis of previous kinetic studies (*29*). The proposed key oxyanion holes, G182−183 and G419′−A420′, are located on two different monomers. Therefore, the dimeric, di-domain interaction and the maintenance of such interactions not only are important for protein stability and substrate recognition but also should be a requirement for the enzyme catalysis of biotin-dependent CTs.

It should be mentioned that an acid-catalyzed mechanism should be chemically feasible, namely, N1 of biotin can be protonated, followed by the attack of C-α on CO_2 and the release of biotin (a very good leaving group). This mechanism has been observed previously for carboxybiotin, carboxyimidazolidone, and carbamates (*29*) and requires a proton source and the base for a C-α proton. Since we could not identify both requirements in the active site, we propose the mechanism in Figure 5. Alternatively, the carboxyl group attached to biotin may also act as the active site base for the C-α proton, although its pK_a does not match as well that of the C-α proton as that of N1 of biotin. Finally, we should caution that the mechanism outlined in Figure 5 is based on the cocrystal structure of biotin with propionyl-CoA, which is not a productive substrate pair (biotin with methylmalonyl-CoA or carboxylbiotin with propionyl-CoA). However, the location of two oxyanion holes strongly supports the charge development during the catalysis.

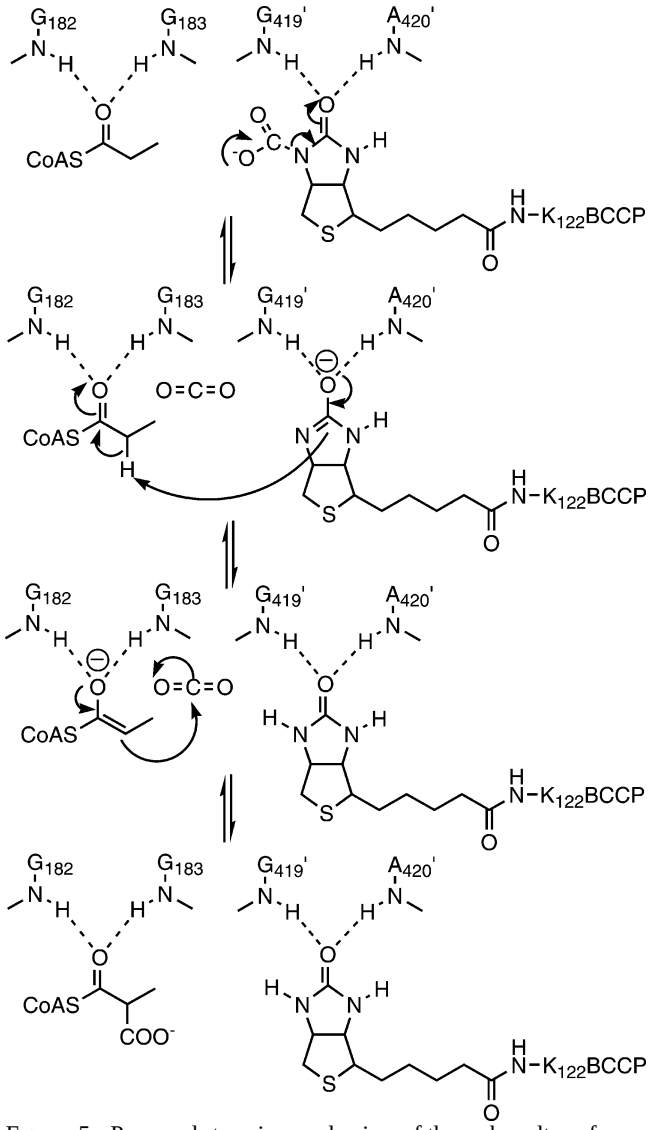

FIGURE 5: Proposed stepwise mechanism of the carboxyltransferase such as PccB and AccB. Once the biotin−carboxyl moiety has bound, CO_2 release can be stabilized by the oxyanion hole at G182 and G183, while the resulting ureido enolate in biotin can be stabilized by the oxyanion hole at G419′ and A420′. With N1 of biotin acting as the active site base, subsequent deprotonation of the α-carbon of propionyl-CoA results in the propionyl enolate, which can be stabilized by the G419′−G420′ oxyanion hole. The attack of the propionyl enolate on CO_2 then produces the product methylmalonyl-CoA.

In conclusion, on the basis of the crystal structures of both apo and substrate-bound PccB, we were able to locate the

binding pockets for both the biotin and the acyl-CoA. Our results indicate the ubiquitous importance of the dimeric, di-domain interaction for the stability, enzyme catalysis, and substrate recognition of biotin-dependent carboxyltransferases. Significantly, on the basis of the crystal structure and sequence comparison, we were able to interconvert the substrate specificity of ACC and PCC complexes by a single mutation (residue 422). The crystal structures reported here have shed light on the molecular basis of substrate recognition and the remarkable architecture of the entire ACCase assembly (presumably $\alpha_6\beta_6\epsilon_{>6}$). This, in turn, will be of great help to computer-aided drug design targeted at the active site of AccB and PccB as candidates of cancer, diabetes, and obesity therapeutics. Finally, our findings have located the active site residues that can be mutated to alter the ACCase substrate specificity, which provides the basis for engineering "new" enzyme complexes with optimized biochemical properties according to the chemical structure of the polyketide of interest.

ACKNOWLEDGMENT

We thank Prof. Vivien Yee and Prof. Liang Tong for their generous provision of the atomic coordinates of 12S and yeast-CT.

REFERENCES

1. Dakshinamurti, K., and Chauhan, J. (1988) Regulation of biotin enzymes, *Annu. Rev. Nutr. 8*, 211−233.
2. Cronan, J. E., Jr., and Waldrop, G. L. (2002) Multi-subunit acetyl-CoA carboxylases, *Prog. Lipid Res. 41*, 407−435.
3. Cane, D. E., Walsh, C. T., and Khosla, C. (1998) Harnessing the biosynthetic code: combinations, permutations, and mutations, *Science 282*, 63−68.
4. Milgraum, L. Z., Witters, L. A., Pasternack, G. R., and Kuhajda, F. P. (1997) Enzymes of the fatty acid synthesis pathway are highly expressed in in situ breast carcinoma, *Clin. Cancer Res. 3*, 2115−2120.
5. Pacheco-Alvarez, D., Solorzano-Vargas, R. S., and Del Rio, A. L. (2002) Biotin in metabolism and its relationship to human disease, *Arch. Med. Res. 33*, 439−447.
6. Witters, L. A., Widmer, J., King, A. N., Fassihi, K., and Kuhajda, F. (1994) Identification of human acetyl-CoA carboxylase isozymes in tissue and in breast cancer cells, *Int. J. Biochem. 26*, 589−594.
7. Mandrup, S., Loftus, T. M., MacDougald, O. A., Kuhajda, F. P., and Lane, M. D. (1997) Obese gene expression at in vivo levels by fat pads derived from s.c. implanted 3T3-F442A preadipocytes, *Proc. Natl. Acad. Sci. U.S.A. 94*, 4300−4305.
8. Pizer, E. S., Thupari, J., Han, W. F., Pinn, M. L., Chrest, F. J., Frehywot, G. L., Townsend, C. A., and Kuhajda, F. P. (2000) Malonyl-coenzyme-A is a potential mediator of cytotoxicity induced by fatty-acid synthase inhibition in human breast cancer cells and xenografts, *Cancer Res. 60*, 213−218.
9. Levert, K. L., Waldrop, G. L., and Stephens, J. M. (2002) A biotin analog inhibits acetyl-CoA carboxylase activity and adipogenesis, *J. Biol. Chem. 277*, 16347−16350.
10. Diacovich, L., Peiru, S., Kurth, D., Rodriguez, E., Podesta, F., Khosla, C., and Gramajo, H. (2002) Kinetic and structural analysis of a new group of Acyl-CoA carboxylases found in *Streptomyces coelicolor* A3(2), *J. Biol. Chem. 277*, 31228−31236.
11. Haase, F. C., Beegen, H., and Allen, S. H. (1984) Propionyl-coenzyme A carboxylase of *Mycobacterium smegmatis*. An electron microscopic study, *Eur. J. Biochem. 140*, 147−151.
12. Hunaiti, A. R., and Kolattukudy, P. E. (1982) Isolation and characterization of an acyl-coenzyme A carboxylase from an erythromycin-producing *Streptomyces erythreus*, *Arch. Biochem. Biophys. 216*, 362−371.
13. Kimura, Y., Kojyo, T., Kimura, I., and Sato, M. (1998) Propionyl-CoA carboxylase of *Myxococcus xanthus*: catalytic properties and function in developing cells, *Arch. Microbiol. 170*, 179−184.
14. Rodriguez, E., Banchio, C., Diacovich, L., Bibb, M. J., and Gramajo, H. (2001) Role of an essential acyl coenzyme A carboxylase in the primary and secondary metabolism of *Streptomyces coelicolor* A3(2), *Appl. Environ. Microbiol. 67*, 4166−4176.
15. Rodriguez, E., and Gramajo, H. (1999) Genetic and biochemical characterization of the α and *β* components of a propionyl-CoA carboxylase complex of *Streptomyces coelicolor* A3(2), *Microbiology 145* (Part 11), 3109−3119.
16. Pfeifer, B. A., Admiraal, S. J., Gramajo, H., Cane, D. E., and Khosla, C. (2001) Biosynthesis of complex polyketides in a metabolically engineered strain of *E. coli*, *Science 291*, 1790−1792.
17. Jitrapakdee, S., and Wallace, J. C. (2003) The biotin enzyme family: conserved structural motifs and domain rearrangements, *Curr. Protein Pept. Sci. 4*, 217−229.
18. Zhang, H., Yang, Z., Shen, Y., and Tong, L. (2003) Crystal structure of the carboxyltransferase domain of acetyl-coenzyme A carboxylase, *Science 299*, 2064−2067.
19. Wendt, K. S., Schall, I., Huber, R., Buckel, W., and Jacob, U. (2003) Crystal structure of the carboxyltransferase subunit of the bacterial sodium ion pump glutaconyl-coenzyme A decarboxylase, *EMBO J. 22*, 3493−3502.
20. Hall, P. R., Wang, Y. F., Rivera-Hainaj, R. E., Zheng, X., Pustai-Carey, M., Carey, P. R., and Yee, V. C. (2003) Transcarboxylase 12S crystal structure: hexamer assembly and substrate binding to a multienzyme core, *EMBO J. 22*, 2334−2347.
21. Holden, H. M., Benning, M. M., Haller, T., and Gerlt, J. A. (2001) The crotonase superfamily: divergently related enzymes that catalyze different reactions involving acyl coenzyme a thioesters, *Acc. Chem. Res. 34*, 145−157.
22. Benning, M. M., Taylor, K. L., Liu, R. Q., Yang, G., Xiang, H., Wesenberg, G., Dunaway-Mariano, D., and Holden, H. M. (1996) Structure of 4-chlorobenzoyl coenzyme A dehalogenase determined to 1.8 Å resolution: an enzyme catalyst generated via adaptive mutation, *Biochemistry 35*, 8103−8109.
23. Benning, M. M., Haller, T., Gerlt, J. A., and Holden, H. M. (2000) New reactions in the crotonase superfamily: structure of methylmalonyl CoA decarboxylase from *Escherichia coli*, *Biochemistry 39*, 4630−4639.
24. Bahnson, B. J., Anderson, V. E., and Petsko, G. A. (2002) Structural mechanism of enoyl-CoA hydratase: three atoms from a single water are added in either an E1cb stepwise or concerted fashion, *Biochemistry 41*, 2621−2629.
25. Modis, Y., Filppula, S. A., Novikov, D. K., Norledge, B., Hiltunen, J. K., and Wierenga, R. K. (1998) The crystal structure of dienoyl-CoA isomerase at 1.5 Å resolution reveals the importance of aspartate and glutamate side chains for catalysis, *Structure 6*, 957−970.
26. Otwinoswski, Z., and Minor, W. (1997) Processing of X-ray Diffraction Data Collected in Oscillation Mode, *Methods Enzymol. 276*, 307−326.
27. Brunger, A. T., Adams, P. D., Clore, G. M., DeLano, W. L., Gros, P., Grosse-Kunstleve, R. W., Jiang, J. S., Kuszewski, J., Nilges, M., Pannu, N. S., Read, R. J., Rice, L. M., Simonson, T., and Warren, G. L. (1998) Crystallography & NMR system: A new software suite for macromolecular structure determination, *Acta Crystallogr. D54* (Part 5), 905−921.
28. Schwede, T., Kopp, J., Guex, N., and Peitsch, M. C. (2003) SWISS-MODEL: An automated protein homology-modeling server, *Nucleic Acids Res. 31*, 3381−3385.
29. Knowles, J. R. (1989) The mechanism of biotin-dependent enzymes, *Annu. Rev. Biochem. 58*, 195−221.
30. Lindqvist, Y., and Schneider, G. (1996) Protein-biotin interactions, *Curr. Opin. Struct. Biol. 6*, 798−803.
31. Yong-Biao, J., Islam, M. N., Sueda, S., and Kondo, H. (2004) Identification of the catalytic residues involved in the carboxyl transfer of pyruvate carboxylase, *Biochemistry 43*, 5912−5920.
32. Cronan, J. E., Jr. (2001) The biotinyl domain of *Escherichia coli* acetyl-CoA carboxylase. Evidence that the "thumb" structure is essential and that the domain functions as a dimer, *J. Biol. Chem. 276*, 37355−37364.
33. Smith, G. R., and Sternberg, M. J. (2003) Evaluation of the 3D-Dock protein docking suite in rounds 1 and 2 of the CAPRI blind trial, *Proteins 52*, 74−79.
34. Blanchard, C. Z., and Waldrop, G. L. (1998) Overexpression and kinetic characterization of the carboxyltransferase component of acetyl-CoA carboxylase, *J. Biol. Chem. 273*, 19140−19145.

BI049065V